

Unveiling migration mechanisms of Mg and Sc atoms at ScAlMgO₄-GaN interfaces

Yueping Hu^a, Weifang Lu^{a,b,*}, Jinjian Yan^a, Yang Sun^a, Guangyang Lin^a, Wei Huang^a, Kai Huang^{a,b}, Cheng Li^a, Satoshi Kamiyama^c, Songyan Chen^a

^a College of Physical Science and Technology Xiamen, University, Xiamen 361005, China

^b Future Display Institute of Xiamen, Xiamen 361005, China

^c Department of Materials Science and Engineering, Meijo University, 1-501 Shiogamaguchi, Tempaku-ku, Nagoya 468-8502, Japan

ARTICLE INFO

Keywords:
ScAlMgO₄ (SAM)
GaN
Surface energy
Interface energy
Formation energy
Energy band

ABSTRACT

The structures and stability of ScAlMgO₄ (SAM)-GaN interface are systematically investigated via first-principles calculations. The mechanisms by which Mg and Sc atoms diffuse into GaN from the SAM substrate under different structural configurations are studied. Energy calculations identified the Sc-O-terminated surface as the most stable one for SAM, followed by a configuration with one Mg(Al)-O layer above the Sc-O layer. Interfacial energy calculations revealed distinct preferences for GaN growth polarity: the Sc-O surface favors bonding with Ga atoms, leading to N-polar GaN growth, while the Mg-O surface preferentially bonds N atoms, resulting in Ga-polar growth. Defect formation energy analysis shows Mg and Sc atoms do not readily diffuse individually from SAM into GaN. In the Sc-O terminated structure, Mg can occupy six-coordinated interstitial sites within GaN under excess Mg conditions. For Sc atoms, direct diffusion through the interface into GaN is also unlikely. However, in the Mg-O terminated structure, dissociated Sc atoms in interfacial region can bind to interstitial sites within GaN, a behavior absent in the Sc-O terminated structure. These findings highlight the critical role of interfacial structure in controlling of Mg and Sc doping, which is crucial for the growth of lattice-matched GaN on SAM. Electronic structure analyses of Mg- or Sc-doped GaN under experimentally relevant concentrations revealed that Sc diffusion into interstitial sites reduces the GaN bandgap, potentially shifting its emission toward longer wavelengths. This study provides insights into precise control of Sc and Mg atoms at SAM-GaN interfaces, offering a pathway for optimizing the electronic and optical properties of GaN grown on SAM substrates.

1. Introduction

In recent years, micro-light-emitting diodes (micro-LEDs) have emerged as a cutting-edge display technology, meeting the high-resolution demands of near-eye displays such as virtual reality and augment reality [1,2]. At the core of this technology are III-nitride semiconductors, which offer the potential for full-spectrum visible light emission and are traditionally grown on sapphire or Si substrates [3–6]. However, the lattice mismatch and thermal expansion differences between GaN and foreign substrates lead to high dislocation density, cracks, and wafer bowing during heteroepitaxial growth [7]. To address these issues, one promising candidate is ScAlMgO₄ (SAM), which exhibits a lattice mismatch of 1.8 % with GaN—a substantial improvement compared to that with sapphire (16 %) [8,9]. Additionally, the coefficient of thermal expansion mismatch between GaN and SAM is 10.9 %

[10], which is also lower than that between GaN and sapphire (27 % [11]). Various epitaxial methods, including metalorganic vapor phase epitaxy (MOVPE) [12–15], pulse laser deposition [16,17], hydride vapour-phase epitaxy [7,18], and molecular beam epitaxy (MBE) [19], have been successfully applied to grow high-quality (In)GaN and GaInN/GaN multiple quantum well structures on SAM substrates [12, 20].

SAM substrates demonstrate great potential for growing GaInN layers capable of achieving high-efficiency red luminescence. However, several challenges remain in optimizing the epitaxial growth of (In)GaN on SAM substrates. Recent studies have found significant incorporation of impurities in the initial n-GaN epilayers grown directly on SAM substrates, with Mg and Sc concentrations exceeding $5 \times 10^{18} \text{ cm}^{-3}$ and $1 \times 10^{15} \text{ cm}^{-3}$, respectively [7,21]. The uncontrolled doping of Mg not only compensates the n-type conductivity of GaN but also promotes the

* Corresponding author.

E-mail addresses: weilu.weif@xmu.edu.cn (W. Lu), yangsun@xmu.edu.cn (Y. Sun), sychen@xmu.edu.cn (S. Chen).

formation of extended defects such as inversion domain boundaries and Mg-enriched clusters, which can degrade the crystal quality and adversely impact carrier injection efficiency of LED devices [22–25]. In wurtzite GaN, high-concentration Mg doping with levels exceeding $2 \times 10^{19} \text{ cm}^{-3}$ results in blue luminescence due to strong donor-acceptor pair (DAP) emission [26], while in zincblende GaN, blue luminescence has also been observed at Mg doping concentrations exceeding $4 \times 10^{19} \text{ cm}^{-3}$ [27]. This phenomenon not only hinders precise control of emission properties but also presents significant challenges for achieving GaInN-based red light emission. Therefore, it is crucial to precisely control the Mg doping level, specifically in the n-GaN epilayers during growth on SAM substrates. The impact of Sc doping on the electronic properties of GaN remains unresolved, with no definitive conclusions drawn from theoretical or experimental studies. Notably, photoluminescence (PL) measurements of Sc-doped GaN showed a luminescence peak at 580 nm [28]. However, whether Sc doping directly contributes to this red-shift has not been conclusively determined, which is of great significance for the realization of GaN-based red LEDs. Moreover, the diffusion behavior of Sc from SAM into GaN needs further investigation, as it may influence both the material's structural and optical properties.

The presence of Mg and Sc atoms in (In)GaN epilayers is attributed to two possible mechanisms. First, these atoms in SAM may diffuse directly into GaN during the high-temperature epitaxy process. Alternatively, the SAM substrate may partially cleave and decompose into the growth chamber during high-temperature thermal cleaning prior to growth, allowing Mg and Sc to incorporate as impurities during the growth of GaN [29] or InGaN [30] layers. Despite these hypotheses, the mechanism of doping is not yet fully understood. Currently, low-temperature (In)GaN buffer layer [7,12,18,20,31–35] or AlInN underlying layer [36] which can effectively suppress Mg impurity contamination from the SAM substrate has been attempted. Since the decomposition occurs from the surface, sidewall, and back of the SAM substrate, additional protective materials such as SiO₂ [31], Ti [15], and AlN [14,36,37] were applied to clad the decomposition-prone SAM substrates. Recent observations of atomic arrangement near the interface strongly suggest that N-polar GaN grows preferentially on the Sc–O surface of SAM [13, 14,38]. While there have been experiments growing Ga-polar GaN on SAM, direct characterizations of the atomic structure at the interface are lacking [15,17,39]. First-principles calculations indicate that the growth polarity is influenced by the surface composition of SAM: Ga-polar GaN predominantly forms on the Mg(Al)–O surface, whereas N-polar GaN is typically realized on the Sc–O surface [17,40]. However, molecular dynamics mechanisms of how Mg and Sc from SAM substrates integrate into GaN or InGaN epilayers during growth have not been reported yet. A thorough investigation into the atomic-scale dynamics at the interface, particularly the role of Mg and Sc, could provide valuable insights into defect formation, interface stability, and growth polarity control.

In this work, we systematically explored the mechanisms of Mg and Sc atoms into GaN from SAM using density-functional theory (DFT) to uncover novel insights into growth polarity, interfacial stability, and doping control. Prior to delving into the specifics of diffusion, the surface energy of various configurations on SAM was calculated to identify the most stable surface of SAM for growth. Subsequently, we constructed GaN-on-SAM heterostructures and calculated interface energies for various arrangements to determine the optimal configuration. Based on the optimal configuration, the formation energies of potential defects were investigated to assess their likelihood of formation. Additionally, we calculated the electronic structure of a series of Mg/Sc-doped GaN with concentrations consistent with the experimental results.

This study contributes to the field of surface and interface science by elucidating the atomic-scale dynamics of impurity diffusion and interfacial bonding at SAM-GaN interfaces. Our findings provide a comprehensive framework for optimizing the growth of GaN on SAM substrates, offering key insights into the mechanisms governing doping levels, defect formation, and growth polarity, which are critical for achieving

precise control over these parameters. These insights are critical for improving the performance of GaN-based devices, especially in applications like micro-LEDs and full-spectrum visible light emission. By bridging the gap between theoretical predictions and experimental observations, this work not only enhances our understanding of SAM-GaN interfaces but also paves the way for the development of next-generation optoelectronic devices with tailored electronic and optical properties.

2. Calculation method

To investigate the diffusion mechanism of Mg and Sc from SAM substrate to GaN, first-principles calculations were performed using the Vienna ab initio simulation package (VASP) software based on DFT [41, 42]. The projector-augmented wave (PAW) method was used to describe the interactions between ions and valence electrons. The Perdew-Burke-Ernzerhof (PBE) exchange-correlation functional, a specific implementation of the generalized gradient approximation (GGA), was employed for accurate energy calculations [43]. A plane-wave cutoff energy of 520 eV was utilized throughout the simulations to ensure calculation accuracy. Different slab models were constructed to simulate the surface properties, interfacial interactions, and defect distributions. The Monkhorst-Pack grids of $4 \times 4 \times 1$ and $6 \times 6 \times 1$ k-points were applied for sampling the Brillouin zone of the SAM slab model and heterogeneous interface slab model, respectively. To eliminate the interaction between adjacent supercells caused by periodicity, a vacuum layer of at least 12 Å was introduced along the vertical direction of the slab models. For all calculations, the geometries of ions were optimized using the conjugate gradient algorithm with energy convergence set at 1×10^{-4} eV.

3. Results and discussion

3.1. Surface properties of SAM

To calculate the surface energy of SAM substrate, both 1×1 and 2×2 slab models with vacuum layers of larger than 12 Å were constructed on the top and bottom symmetric and bare surfaces, as shown in Figs. 1 (a) and (b). Different surface configurations with O–Sc, O, O–Mg, O–O, Mg–O, Mg, Sc–O terminations were calculated, denoted as OSc, O, OMg, OO, MgO, Mg, and ScO, respectively. As referred to the literature, the calculations of the surface energies of SAM were carried out using the following formula through the first-principles calculation [17]:

$$E_{\text{surface}} = \frac{E_{\text{slab}} - E_{\text{bulk}}(N_{\text{slab}}/N_{\text{bulk}})}{2A} \quad (1)$$

where, the total energy of the slab is represented by E_{slab} , and E_{bulk} represents the primary cell energy of bulk SAM. N_{slab} is the total number of atoms in the slab model, and N_{bulk} is the number of atoms corresponding to the primary cell of bulk SAM. In addition, the A represents one surface area of the bare slab.

The calculated surface energy values of the SAM with O–Sc, O, O–Mg, O–O, Mg–O, Mg, Sc–O terminations are presented in Fig. 1(c). The surface energy calculations for both 1×1 and 2×2 slab models indicate that the Sc–O terminated surface is the most stable, followed by the Mg–O terminated surface. This result is consistent with previous findings reported by Guo et al. [44]. The calculated results of the 1×1 slab model, which is identical to another case reported by Zheng et al. [17], unfortunately diverged from the literature results. It is conceivable that other researchers employed a different symmetric slab model from the one used in this work. It is noteworthy that the MgO-terminated surface (with a single MgO layer on the ScO layer) exhibits higher stability than the OMg-terminated surface (with two MgO layers on the ScO layer). This stability difference arises from the distinct structural configurations: each MgO layer inherently forms tetrahedral units resembling the wurtzite-type structure, while the interlayer bonding between

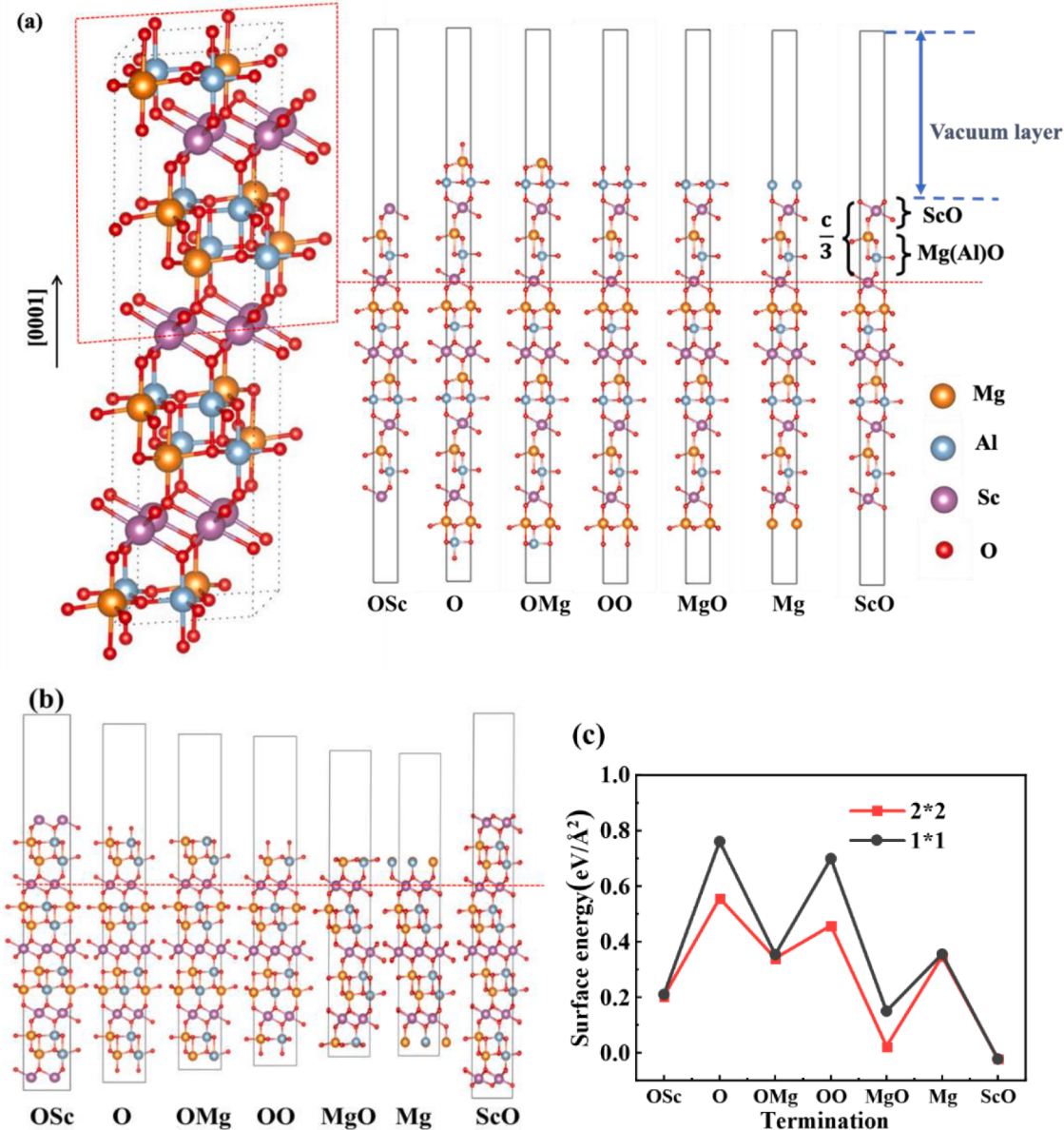


Fig. 1. (a) 1×1 and (b) 2×2 slab models of the seven different stoichiometric terminal surfaces of ScAlMgO_4 (SAM) (denoted from left to right as OSc, O, OMg, OO, MgO, Mg, and ScO, respectively). (c) Surface energy as a function of different terminal surfaces of SAM in 1×1 model (black line) and 2×2 model (red line).

adjacent MgO layers is weak. This conclusion is consistent with the structural analysis reported by Hanada et al. [29] and further supported by the bond length distributions in bulk SAM derived from our calculations (see Supporting Information Figure S1 and Table 1). Notably, the tetrahedral coordination in individual Mg(Al)O layers shows bond lengths of $1.76\text{--}1.84$ Å for $\text{Al}-\text{O}$ and $1.96\text{--}2.05$ Å for $\text{Mg}-\text{O}$, consistent with wurtzite-like configurations. In contrast, the interlayer $\text{Al}-\text{O}$ distances exceed 2.25 Å, and the interlayer $\text{Mg}-\text{O}$ distances are larger than 2.12 Å, indicating a lack of strong covalent interactions. These findings pave the way for further analysis, where the surface energies obtained for the 2×2 slab configuration were applied in the subsequent calculations, propelling the understanding of interface properties of GaN-on-SAM and the dynamic behaviors of the defects in the epilayers on SAM.

3.2. Interface stabilities of GaN-ON-SAM

Based on the aforementioned findings, the $\text{Sc}-\text{O}$ and $\text{Mg}-\text{O}$ surfaces with the lowest surface energy in this work, as well as the reported

$\text{O}-\text{Mg}$ surface with the lowest surface energy [17], were considered as the terminal facets of the (0001) -plane SAM to constitute a heterogeneous interface with GaN epilayer, characterized by Ga/N polarity and Ga/N terminals. To construct the 2×2 slab model, as illustrated in Fig. 2 (a), a vacuum layer of 12 Å was introduced. Each slab consists of three stoichiometric units of a SAM layer, along with five layers of GaN. Within the SAM layer, a single stoichiometric unit follows the sequence of $-\text{O}-\text{Sc}-\text{O}-\text{Mg}/\text{Al}-\text{O}-\text{O}-\text{Mg}/\text{Al}-$, resulting in a protocell containing precisely three such units. To maintain the surface integrity and prevent surface disorder, the first layer of GaN was fixed due to the strong polarity of GaN. The interfacial energy between the SAM and the GaN was calculated using Eq. (2):

$$\sigma_{int} = \frac{E_{total} - E_{bulkGaN} - E_{bulkSAM} - A\sigma_{surfGaN} - A\sigma_{surfSAM}}{A} \quad (2)$$

Here, E_{total} and A represent the total energy and the cross-section area of the 2×2 slab, respectively. $E_{bulkGaN}$ denotes the energy of five layers of GaN in bulk, while $E_{bulkSAM}$ represents the energy of a 2×2 protocell SAM in bulk. Additionally, $\sigma_{surfGaN}$ and $\sigma_{surfSAM}$ are the surface energies

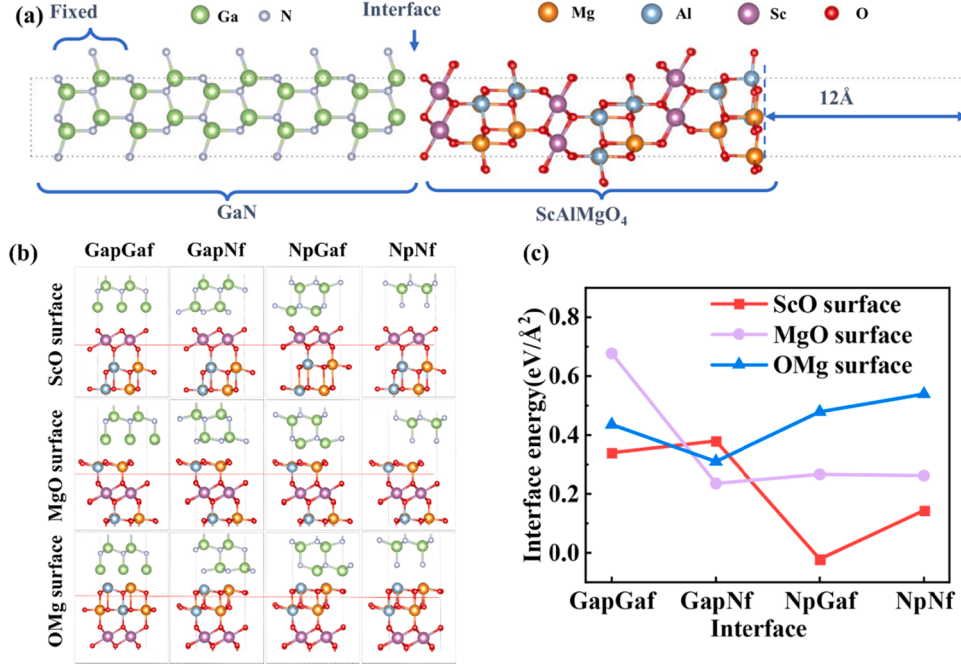


Fig. 2. (a) Schematic diagram of the slab model; (b) Schematic illustration of possible atomic arrangements at the interface between GaN (with Ga/N polarity and Ga/N terminals) and SAM (with ScO, MgO, and OMg surfaces). (c) Interface energies for the ScO face (red line), MgO face (purple line), and OMg face (blue line) of SAM when paired with the Ga-polar Ga face (GapGaf), Ga-polar N face (GapNf), N-polar Ga face (NpGaf), and N-polar N face (NpNf), respectively.

of the GaN and SAM exposed to vacuum, respectively. The surface energy values for GaN, derived from the previous literature calculations, are 0.091 eV/Å² for Ga polarity and 0.116 eV/Å² for N polarity [45]. The surface energy of SAM exposed to vacuum has been calculated in previous section. Schematic illustrations of various different heterojunction interfaces are shown in Fig. 2(b). The results reveal that the formation of Ga–O, Sc–N, and Mg(Al)–N bonds at the interface are in these low-energy models. The calculated interface energies are depicted in Fig. 2(c), providing insights into the stability and dynamics of GaN-on-SAM structures.

As depicted in Fig. 2(c), the interface energy analysis highlights the stability of different GaN-on-SAM structures. Lower interface energy indicates a more stable interface, with the Sc–O surface of SAM demonstrating exceptional stability when paired with N-polar Ga-face GaN. This configuration achieves an extremely low interface energy of approximately ~0 eV/Å², which is consistent with the experimental

findings as reported by Najmi et al. [38]. Conversely, the Mg–O surface of SAM demonstrates a preference for GaN with Ga polar and N face, although direct experimental characterization of this atomic-scale interface remains lacking. However, its interface energy is approximately 0.2 eV/Å² higher than that with Sc–O surface. Furthermore, the difference in interface energy at the Mg–O surface of SAM between the Ga-polar N-face and N-polar Ga-face is minimal, at approximately 0.03 eV/Å². Notably, the interface between the MgO surface of SAM and the N surface of Ga-polar GaN exhibits relatively higher interface energy compared to the ScO surface, indicating a less stable configuration.

From the atomic interfaces observed after relaxation (refer to Fig. 3), it can be found that the stability of the heterogeneous interface between the Sc–O face of SAM and the Ga face of N-polar GaN is primarily attributed to the formation of stable Ga–O bonds at the interface, with a bond length of 1.958 Å. However, at the Mg–O face of SAM, Ga–O and Mg(Al)–N double bonds do form, but their relatively long bond lengths

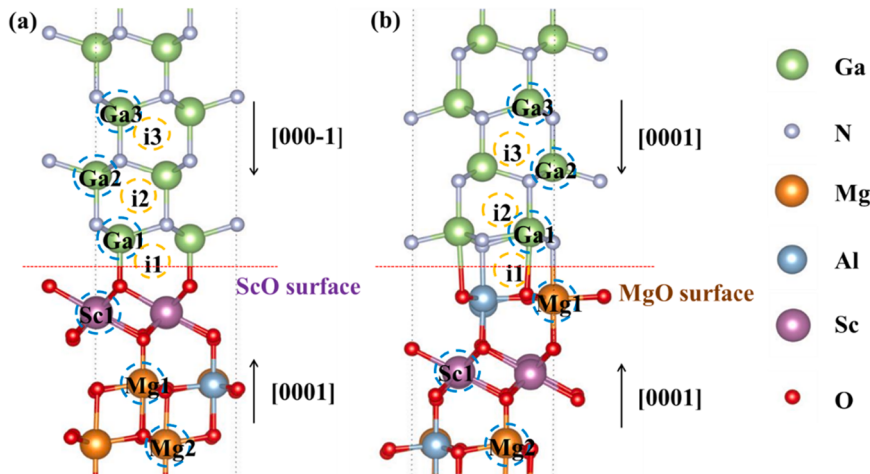


Fig. 3. Schematics of the stable heterogeneous interfaces formed by the (a) Sc–O face of SAM and the Ga face of N-polar GaN (referred as SCO structure); (b) Mg–O face of SAM with N face of Ga-polar GaN (referred as MGO structure).

of 2.83 Å for Ga–O and Al–N, and 2.3 Å for Mg–N, resulting in weaker bonding interactions. These bond lengths are comparable to the Mg(Al)–O double bond in SAM [29]. Although double-density bonding is present, the weakened strength of the bonds due to the longer bond lengths reduces the effectiveness of this bonding arrangement. Consequently, the interface energy between the Mg–O face of the SAM and the N face of the Ga-polar GaN is substantially higher, leading to an unstable interface.

3.3. Defect distribution properties in GaN-ON-SAM heterostructures

To investigate the doping of Mg and Sc atoms in GaN, which originate from SAM, the formation energies of various defects were calculated. Two stable interfaces were considered: Ga-face of N-polar GaN on the Sc–O surface of SAM and N-face of Ga-polar GaN on the Mg–O surface of SAM, later referred to as the SCO structure and the MGO structure, as is shown in Figs. 3(a) and (b).

The defect formation energies were calculated using Eq. (3) [46].

$$E_f = E_D - E_p - \sum n_i \mu_i \quad (3)$$

Here, E_f is the formation energy, E_D is the total energy of the model containing defects, E_p is the total energy of the defect-free model, μ_i is the atomic chemical potential of the defective atom i , and n_i is the number of atoms i added to or removed from the defect-free model (addition is positive, removal is negative). The formation energy provides a measure of how easily a defect can form under specific conditions. Defect concentration follows the Boltzmann distribution $c = N_{\text{exp}} (-E_f/k_B T)$, where the exponential term represents the probability of defect formation during thermal activation [47]. For typical GaN growth temperatures around 1300 K, this corresponds to a thermal excitation energy of 0.11 eV($k_B T$). Defects with formation energies lower than the typical GaN growth temperature activation energy of approximately 0.11 eV are more likely to form, as they can be activated by the thermal energy available during growth. Conversely, defects with formation energies higher than 0.11 eV are less likely to form, as they require more energy than is available at typical growth temperatures. But this value corresponds to a high defect occurrence probability of $c/N = e^{-1} \approx 0.37$. If considering lower defect concentrations, this threshold can be appropriately increased.

3.3.1. Formation energies of Mg-related defects at the interfaces

In both the SCO and MGO structures, we first explored the possibility of Mg direct access to GaN across the GaN-SAM interface. The vacancies are categorized as V_{Mg} for Mg1 and Mg2 in SAM, and V_{Ga} for Ga1, Ga2, and Ga3 in different positions of GaN, as marked in Fig. 4. The antisite defects are labelled as A_{MgGa} for the Mg1-Ga1 pair. Additionally, the migration of Mg1 to the interstitial site i2 is noted as mMg_i . Since the discussion mainly focuses on the distribution of Mg atoms at the

interface and the complexity of the elemental species involved, the formation energies in Mg-rich, Ga-rich, and N-rich cases were investigated, as shown in Fig. 4. The corresponding chemical potentials of μ_{Mg} , μ_{Ga} , and μ_N , derived from the GaN and Mg_3N_2 system [48], are shown in Table 3 of the Supplementary Information.

According to Fig. 4, the formation of V_{Mg} within SAM region in SCO structure requires an excitation energy of >1 eV in a N-rich atmosphere, making it a challenging process. For MGO structure, the required energy is even higher, exceeding 6 eV. Similarly, the formation of V_{Ga} within 8 Å of the GaN region on the Sc–O surface is highly unlikely, the formation energies increase with distance from the interface, making it more difficult for V_{Ga} to appear further away from the surface. In the MGO structure, vacancies are more easily formed in the Ga1 than in the Ga2 and Ga3 sites. This is attributable to the inherent instability of Ga–O bonds at the interface of MGO structures, as discussed in previous section. However, even in the Ga1 site, formation energy for V_{Ga} remains relatively high, higher than 1 eV. Therefore, the likelihood of vacancies being present in the Mg or Ga sites near the interface appears exceedingly low. Additionally, the calculated formation energies of A_{MgGa} in both the SCO and MGO structures exceed 2 eV and 1 eV, respectively. Even for mMg_i , which is mentioned in some experimental studies [49,50] that Mg is prone to occupy interstitial sites, has a rather high defect formation energy (above 8 eV in the SCO structure and close to 4 eV in the MGO structure). Considering these findings collectively, the direct diffusion of Mg into GaN from the SAM substrate can almost be excluded.

T. Iwabuchi et al. reported that GaN grown on an AlN-covered SAM substrate did not exhibit a lower Mg concentration compared to direct GaN growth on SAM [30]. However, when the SAM substrate was entirely coated, the Mg concentration in grown GaN was effectively reduced. This is consistent with our conclusion that Mg does not diffuse across the SCAM-GaN interface into GaN. It was speculated that the incorporated Mg most likely originates from the partial decomposition of SAM during the high-temperature thermal cleaning process with hydrogen prior to the GaN epitaxial [13,15,38]. The thermal annealing may release Mg atoms from SAM into the growth chamber, which are then unintentionally incorporated into the GaN layer as impurities during subsequent growth. Such hypothesis can also be verified in our calculations, where the formation energies of V_{Mg} on seven terminal surfaces of SAM were calculated, detailed in Table 4 of the Supplementary Material. The results revealed the existence of relatively stable O–Mg surfaces (and O–Sc surfaces) with negative formation energies under N-rich conditions. It suggests a high susceptibility of Mg atoms to enter the reaction chamber from the SAM, with the potential to detach in a layered manner, as demonstrated in experiments [21]. However, the precise mechanism near the heterogeneous interface remains unclear, particularly regarding whether Mg atoms preferentially occupy the Ga site (Mg_{Ga}) or instead reside at the classical six-coordination interstitial gap sites (Mg_i) in GaN [49]. To delve deeper insight into this issue,

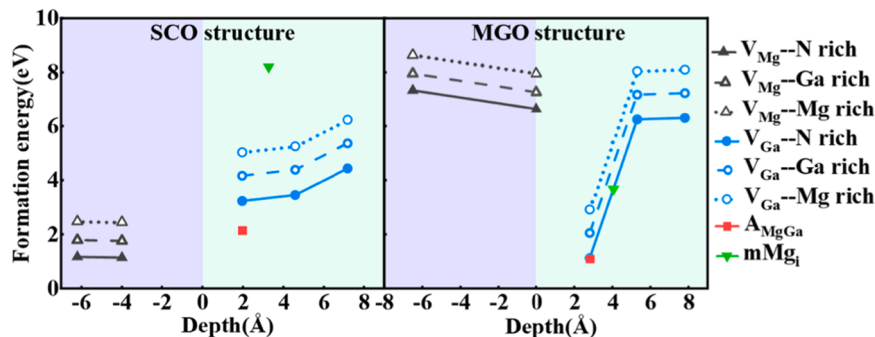


Fig. 4. Formation energies of defects as a function of depth near the SAM-GaN interfaces. The coordinate system is defined such that the interface is at zero, with positive coordinates representing the GaN region and negative coordinates corresponding to the SAM region. V_{Mg} refers to Mg vacancies, V_{Ga} to Ga vacancies, A_{MgGa} to Mg–Ga antisites, and mMg_i to the migration of a Mg atom from SAM to the interstitial sites within GaN.

further calculations were carried out in both the SCO and MGO structures, as plotted in Fig. 5.

In the SCO structure shown in Fig. 5, the results indicate that the formation energy for Mg binding at Ga sites is negative, although it increases with the depth within the GaN layer. Conversely, the formation energy of Mg binding at the interstitial sites is approximately 4 eV, which suggests that Mg preferentially binds to Ga sites in the Sc-O structure. Moreover, this binding becomes more favorable as the distance to the interface decreases, making substitutional defects more likely near the interface. In MGO structure, the formation energy for Mg binding at the six-coordinated interstitial sites is negative, with the energy also increasing with depth. However, the formation energy of Mg binding at Ga sites is higher, about 0.8–0.9 eV, making the formation of substitutional defects less likely. This suggests that, in the MGO structure, Mg atoms are more likely to occupy the six-coordinated interstitial sites, rather than substituting Ga atoms. Overall, these findings imply distinct doping mechanisms for Mg in the GaN, with Mg favoring Ga-site substitution in SCO and interstitial binding in MGO.

3.3.2. Formation energies of Sc-related defects at the interfaces

To assess the migration behavior of Sc in both the SCO and MGO structures, various possibilities for Sc migration from the SAM into the GaN layer were systematically investigated. The potential vacancies for Sc are denoted as V_{Sc} , with Sc1 and Sc2 representing two distinct Sc sites in the SAM. Although Sc2 is not shown in Fig. 3, it refers to the second Sc atom starting from the SAM-GaN interface. The antisite defects, where Sc1 occupies either Ga1 or Ga2, are represented as A_{ScGa} . Additionally, we considered the case where Sc1 migrates to the interstitial site i2, denoted as mSc_i . The presence of additional Sc at Ga1, Ga2, or Ga3 is referred to Sc_{Ga} , while Sc_i represents the occupation of Sc at interstitial sites i1, i2, or i3. Similar to Section 3.1, the formation energies are calculated for Sc-rich, Ga-rich, and N-rich cases, as shown in Fig. 6. The corresponding values for μ_{Sc} , μ_{Ga} , and μ_N , derived from the GaN and ScN system, are given in Tables 5 of the Supplementary Information.

According to Fig. 6, the formation energies of V_{Sc} , A_{ScGa} , and mSc_i are all greater than 0.11 eV under Sc-rich, Ga-rich, and N-rich cases, indicating that these defects are unlikely to form easily. Notably, additional Sc atoms are prone to occupy hexagonal interstitial sites (Sc_i) in GaN within the MGO structure, which is quite difficult in SCO structure. In addition, the calculated formation energy of Sc_{Ga} exceeds 0.6 eV in both SCO and MGO structures, indicating that Sc atoms face substantial energetic barriers when attempting to directly substitute for Ga. These findings also imply that Sc atoms do not easily diffuse across the interface into GaN under normal conditions. However, in the presence of dissociated Sc in the MOVPE chamber, Sc atoms exhibit a preference for binding to interstitial sites in GaN in the MGO structure. As demonstrated by Araki et al. [19], no diffusion of Mg or Sc was observed in GaN epilayers grown on SAM substrate when thermally cleaning at 800 °C in vacuum and subsequent growth at 650 °C were conducted in the MBE chamber. However, diffusion of Mg and Sc was detected in experiments

that involved a high-temperature thermal cleaning step exceeding 1000 °C in a hydrogen ambient prior to growth in a MOVPE chamber [21]. This elevated temperature treatment in the presence of hydrogen likely leads to the decomposition of the SAM substrates, releasing Mg and Sc into the growth chamber. Meanwhile, the terminal surfaces of the SAM substrates are altered by such high-temperature treatments, further influencing the growth dynamics and impurity incorporation in the GaN epilayers.

3.4. Energy band properties of GaN doped with Mg or Sc

As reported in the literature [30], when GaN is grown on a SAM substrate, approximately 10 % of Mg and 2 % of Sc atoms diffuse into the GaN lattice. In fact, studies on the growth of ScGaN emphasized the challenges in achieving a Sc fraction in GaN exceeding 2 % with MBE [28]. Furthermore, the PL emission peak at 580 nm was also observed in the experiment, which is of particular interest. Therefore, energy band properties of GaN doped by Mg or Sc at the corresponding experimental concentrations were calculated. Specifically, we utilized the HSE06 hybrid functionals, known for its superior accuracy in calculating electronic properties [51]. Here, the fraction of exact exchange in the hybrid functional was set to 0.34 to accurately reproduce a band gap of 3.46 eV for GaN with the experimental value [52]. Based on this calibration, two types of Mg-doped GaN protocells were constructed: Mg_1Ga_7N , where Mg substitutes a Ga site, and Mg_1Ga_8N , where Mg occupies an interstitial site, corresponding to MgN fractions of 12.5 % and 11.1 %, respectively. Similarly, for Sc-doped GaN, two protocell models were developed: $Sc_1Ga_{35}N$, with Sc substituting a Ga atom, and $Sc_1Ga_{36}N$, where Sc resides in an interstitial site, representing ScN fractions of 2.78 % and 2.7 %, respectively. Figs. 7(a)–(e) illustrate the atomic arrangements of these protocells, highlighting the positions of Mg and Sc dopants in both substitutional and interstitial sites. Figs. 7(f)–(j) present the corresponding energy band structures, where the Fermi energy level is consistently set to 0 eV for all models.

Doping Mg or Sc into GaN significantly alters its electronic structure and band properties, with notable differences depending on whether these dopants occupy Ga sites or interstitial sites. In Mg_1Ga_7N , it acts as a p-type dopant by shifting the Fermi energy level from the forbidden band into the valence band, as shown in Fig. 7(g). This substitution also narrows the direct bandgap to 3.29 eV compared to undoped GaN, demonstrating its influence on electronic and optical properties. Conversely, in the case of Mg_1Ga_8N the bandgap increases to 4.31 eV, accompanied by the introduction of impurity levels within the forbidden band, as shown in Fig. 7(h). In this configuration, the Fermi energy level rises into the forbidden band, significantly altering carrier dynamics. For $Sc_1Ga_{35}N$ in Fig. 7(i), the substitution of Ga sites by Sc leads to an increase in the bandgap and density of states relative to the intrinsic GaN, while the Fermi energy level remains largely unchanged. In contrast, interstitial Sc in $Sc_1Ga_{36}N$ reduces the bandgap drop to 2.81 eV, pushing the Fermi energy level into the conduction band and exhibiting a

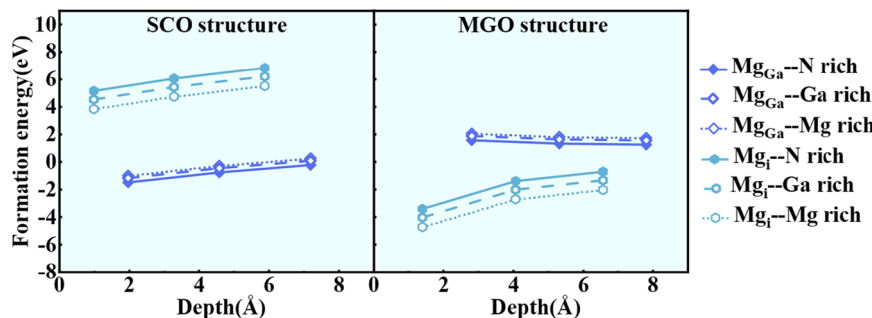


Fig. 5. Formation energies of defects as a function of depth, where the coordinate zero represents the interface and positive coordinates correspond to the GaN region. Mg_{Ga} refers to the Mg atoms occupying the Ga site, while Mg_i represents the additional Mg at the classical six-coordination gap sites.

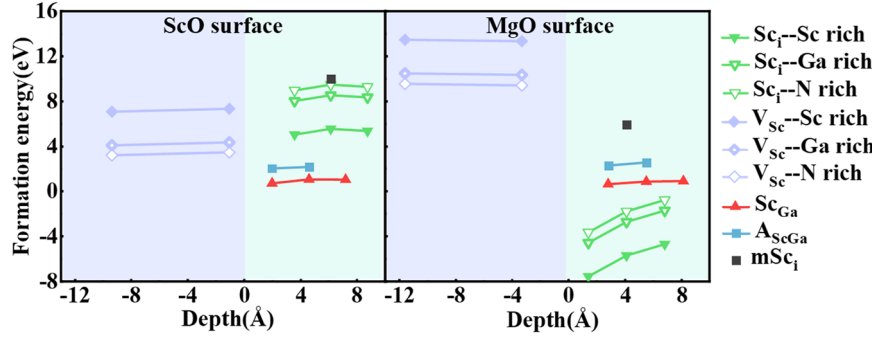


Fig. 6. Formation energies of Sc-related defects as a function of depth, calculated under Sc-rich, Ga-rich, and N-rich cases. The coordinate system is defined such that the interface is at zero, with positive coordinates representing the GaN region and negative coordinates corresponding to the SAM region. V_{Sc} refers to Sc vacancies. A_{ScGa} denotes Sc-Ga antisites. $m\text{Sc}_i$ denotes the movement of a Sc atom from SAM to interstitial sites in GaN. Sc_{Ga} indicates the additional Sc occupying the Ga site. Sc_i refers to the Sc atoms binding at the classical six-coordination interstitial sites.

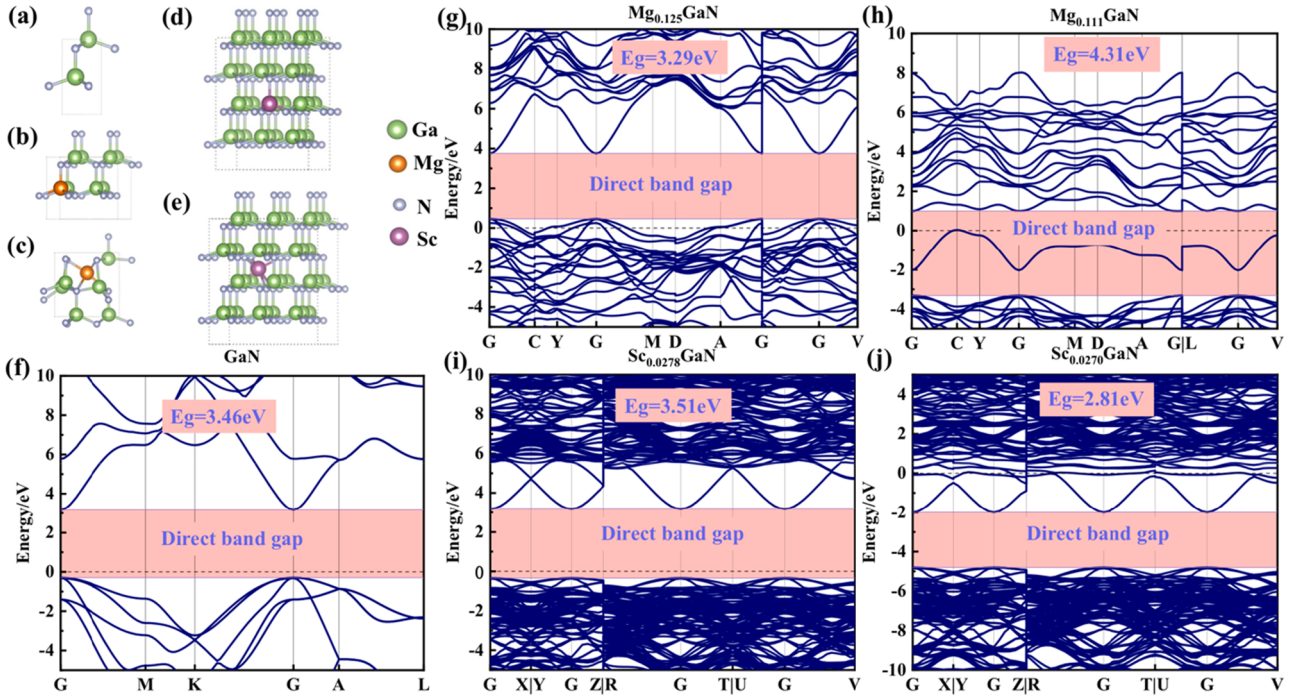


Fig. 7. Protocells of (a) bulk GaN, (b) $\text{Mg}_1\text{Ga}_7\text{N}$ with Mg substitutes a Ga site($\text{Mg}_{0.125}\text{GaN}$), (c) $\text{Mg}_1\text{Ga}_8\text{N}$ with Mg occupies an interstitial site ($\text{Mg}_{0.111}\text{GaN}$), (d) $\text{Sc}_1\text{Ga}_{35}\text{N}$ with Sc substituting a Ga atom ($\text{Sc}_{0.0278}\text{GaN}$), and (e) $\text{Sc}_1\text{Ga}_{36}\text{N}$ with Sc resides in an interstitial site ($\text{Sc}_{0.0270}\text{GaN}$). Corresponding energy band structures of (f) GaN, (g) $\text{Mg}_1\text{Ga}_7\text{N}$, (h) $\text{Mg}_1\text{Ga}_8\text{N}$, (i) $\text{Sc}_1\text{Ga}_{35}\text{N}$, and (j) $\text{Sc}_1\text{Ga}_{36}\text{N}$, respectively.

pronounced metallic character, as shown in Fig. 7(j). Previous mBJ-GGA calculations by Siyuan Zhang et al. on $\text{Sc}_x\text{Ga}_{1-x}\text{N}$ revealed that the hexagonal wurtzite structure (with Sc substituting Ga sites) and a direct bandgap are maintained for $x \leq 0.5$, while the bandgap monotonically increases with rising Sc concentration in the range [53]. Our calculations of $\text{Sc}_1\text{Ga}_{35}\text{N}$ follow this trend, but this is not the case for $\text{Sc}_1\text{Ga}_{36}\text{N}$. Additionally, energy band calculations for interstitial-site doping in ScGaN have not been reported previously. It's the first time to draw the conclusion that Sc doping into the interstitial sites of GaN leads to bandgap reduction. The increase in density of states observed with both Mg and Sc doping highlights their potential to modify properties of GaN for advanced optoelectronic applications. Importantly, the unique effect of interstitial Sc in narrowing the bandgap suggests a promising strategy for achieving redshifts in the emission peaks of GaN-based materials. Despite these promising prospects, the theoretical understanding of Sc doping in GaN remains underexplored. Such calculations are critical to accurately predict electronic structure modifications and guide experimental efforts.

4. Limitations of the present study

The primary limitation of this work is the absence of experimental validation for the computational predictions, highlighting the need for further research. Specifically, atomic-resolution characterization of the GaN-SAM interfaces in Ga-polar GaN systems and defect dynamics during epitaxial growth are essential next steps.

All calculations were performed for identical models once, but additional verification steps were taken to ensure the reliability of the results (See Supplementary Information). Several factors may contribute to potential discrepancies between theory and experiment. **Neglect of Kinetic Barriers:** Only formation energies were considered, while migration barriers were excluded from the models. **Cluster Formation:** Due to the large atomic radius of Sc, vacancy clustering may be favoured over isolated point defects, which was not accounted for in the models. **Charge-State Limitations:** Fermi-level-dependent charge corrections were excluded due to computational complexity involved in large-scale models. **Diffusion Impacts:** The potential effects of Mg/Sc diffusion on

the polarity of GaN film during subsequent growth stages were not considered. **Idealized Assumptions:** The models assumed perfect crystal structures without intrinsic defects in either the SAM or GaN layers, and simplified interface structures by neglecting realistic defect interactions. **Size Effects:** The limited thickness of the slab models may introduce quantum size effects. **Zero-Kelvin Approximation:** The first-principles calculations at 0 K, deviating from the conditions present during actual growth. Addressing these limitations will be beneficial for a more accurate understanding of the GaN-SAM interfaces.

5. Conclusion

The surface energies of SAM with different configurations were calculated using a 2×2 protocell, considering the effects of Mg/Al mixing. The results indicated that the Sc-O terminated surface exhibits the lowest surface energy, making it the most stable, followed by the Mg-O terminated surface. It is uncontroversial that Sc-O terminated surface is the most stable surface, unlike the MgO surface. It is the first study to provide the surface energies of SAM using 2×2 protocells. Based on these findings, various SAM-GaN interfaces were constructed, and their interfacial energies were calculated. Two stable interfaces can be confirmed from the interfacial energies: one composed of the Sc-O surface of SAM with the Ga surface of N-polar GaN, and the other involving the Mg-O surface of SAM with the N-terminated surface of Ga-polar GaN. This is the first time that the stable structure of the GaN-SAM interface has been obtained by interfacial energy calculations. A stable structure on the ScO surface has been observed in experiments, while the other on the MgO surface remains to be verified. To further investigate the interaction between SAM and GaN, the formation energies of defects were calculated for these two stable interfaces, shedding light on the mechanisms by which Mg and Sc diffuse into GaN. It was found that neither Mg nor Sc atoms diffuse individually from the SAM substrate into GaN under typical conditions. For the ScO interface, Mg substitutes Ga atoms in the GaN lattice, while for the MgO interface, Mg occupies six-coordinated interstitial sites within the GaN matrix when Mg concentrations are high in the surrounding MOVPE chamber. As for Sc, Sc also does not readily migrate directly through the interface into GaN. However, in the presence of dissociated Sc within the chamber, Sc atoms are prone to bind to interstitial sites in GaN in the MGO structure, though this is not favored in the SCO structure. Based on stable heterogeneous interfaces, we discussed possible doping pathways for Mg and Sc through defect formation energies. This is a completely new progress that has not yet been proved by direct experimental observations. Finally we calculated the electronic structure and band properties of Mg and Sc in GaN, where doping concentration levels were designed concerning experimental data. Notably, the incorporation of Sc at interstitial sites was found to reduce the bandgap of GaN, potentially contributing to a redshift in emission wavelengths. Not only did we obtain band structure of GaN doped with Mg or Sc atoms at experimental concentrations, but this is also the first time Sc doping into the interstitial sites of GaN has been discussed. This observation provides valuable insights into tuning the optical properties of GaN for advanced optoelectronic applications.

6. Generative AI and figures, images and artwork

The authors declare that we did not use any Generative AI or AI-assisted tools to create or alter images in submitted manuscript.

CRediT authorship contribution statement

Yueping Hu: Writing – original draft, Methodology, Investigation, Formal analysis, Writing – review & editing. **Weifang Lu:** Writing – review & editing, Validation, Supervision, Project administration, Funding acquisition, Formal analysis, Data curation. **Jinjian Yan:** Methodology, Formal analysis, Data curation. **Yang Sun:** Writing –

review & editing, Methodology, Formal analysis, Conceptualization, Funding acquisition. **Guangyang Lin:** Validation, Formal analysis, Methodology, Visualization. **Wei Huang:** Methodology, Data curation, Investigation, Validation. **Kai Huang:** Funding acquisition, Formal analysis, Data curation, Resources, Validation. **Cheng Li:** Resources, Methodology, Data curation, Conceptualization. **Satoshi Kamiyama:** Validation, Supervision, Methodology, Investigation, Conceptualization, Writing – review & editing. **Songyan Chen:** Validation, Supervision, Resources, Methodology, Conceptualization, Writing – review & editing.

Declaration of competing interest

The authors declare that they have no known competing financial interests or personal relationships that could have appeared to influence the work reported in this paper.

Acknowledgement

This work was financially supported by the National Key Research and Development Program of China (Grant No 2022YFB3603604), National Natural Science Foundation of China (Grant No 62404184), and Fundamental Research Funds for the Central Universities (No. 20720230019). Y.S. acknowledges supports from the National Natural Science Foundation of China (Grants Nos. T2422016 and 42374108), the Natural Science Foundation of Xiamen (Grant No 3502Z202371007) and the Fundamental Research Funds for the Central Universities (Grant No 20720230014).

Supplementary materials

Supplementary material associated with this article can be found, in the online version, at [doi:10.1016/j.surfin.2025.106401](https://doi.org/10.1016/j.surfin.2025.106401).

Data availability

Data will be made available on request.

References

- [1] J.-H. Kang, M. Ebaid, J.K. Lee, T. Jeong, S.-W. Ryu, Fabrication of vertical light emitting diode based on thermal deformation of nanoporous GaN and removable mechanical supporter, *ACS. Appl. Mater. Interfaces.* 6 (2014) 8683–8687, <https://doi.org/10.1021/am501406q>.
- [2] Y. Zhang, Q. Sun, B. Leung, J. Simon, M.L. Lee, J. Han, The fabrication of large-area, free-standing GaN by a novel nanoetching process, *Nanotechnology.* 22 (2011) 045603, <https://doi.org/10.1088/0957-4484/22/4/045603>.
- [3] Z. Lu, K. Zhang, J. Zhuang, J. Lin, Z. Lu, Z. Jiang, Y. Lu, Z. Chen, W. Guo, Recent progress of InGaN-based red light emitting diodes, *Micro Nanostructures* 183 (2023) 207669, <https://doi.org/10.1016/j.micra.2023.207669>.
- [4] I. Akasaki, Nobel lecture: fascinated journeys into blue light, *Rev. Mod. Phys.* 87 (2015) 1119–1131, <https://doi.org/10.1103/RevModPhys.87.1119>.
- [5] I.A. Isamu Akasaki, H.A. Hiroshi Amano, Crystal growth and conductivity control of group iii nitride semiconductors and their application to short wavelength light emitters, *Jpn. J. Appl. Phys.* 36 (1997) 5393, <https://doi.org/10.1143/JJAP.36.5393>.
- [6] T. Taki, M. Strassburg, Review—visible leds: more than efficient light, *ECS J. Solid State Sci. Technol.* 9 (2020) 015017, <https://doi.org/10.1149/2.0402001JSS>.
- [7] H. Zhang, S. Takeda, H. Miyake, Growth of thick GaN films on 2-inch ScAlMgO4 substrates by halide vapor phase epitaxy, *J. Cryst. Growth* 625 (2024) 127435, <https://doi.org/10.1016/j.jcrysgro.2023.127435>.
- [8] E.S. Hellman, C.D. Brandle, L.F. Schneemeyer, D. Wiesmann, I. Brener, T. Siegrist, G.W. Berkstresser, D.N.E. Buchanan, E.H. Hartford, ScAlMgO4: an oxide substrate for GaN epitaxy, *MRS Int. J. Nitride Semiconduct. Res.* 1 (1996) 1, <https://doi.org/10.1557/S1092578300001733>.
- [9] W.A. Melton, J.I. Pankove, GaN growth on sapphire, *J. Cryst. Growth* 178 (1997) 168–173, [https://doi.org/10.1016/S0022-0248\(97\)00082-1](https://doi.org/10.1016/S0022-0248(97)00082-1).
- [10] R. Simura, K. Sugiyama, A. Nakatsuka, T. Fukuda, High-temperature thermal expansion of ScAlMgO4 for substrate application of GaN and ZnO epitaxial growth, *Jpn. J. Appl. Phys.* 54 (2015) 075503, <https://doi.org/10.7567/JJAP.54.075503>.
- [11] T. Kozawa, T. Kachi, H. Kano, H. Nagase, N. Koide, K. Manabe, Thermal stress in GaN epitaxial layers grown on sapphire substrates, *J. Appl. Phys.* 77 (1995) 4389–4392, <https://doi.org/10.1063/1.359465>.

- [12] T. Ozaki, Y. Takagi, J. Nishinaka, M. Funato, Y. Kawakami, Metalorganic vapor phase epitaxy of GaN and lattice-matched InGaN on ScAlMgO₄ (0001) substrates, *Appl. Phys. Express.* 7 (2014) 091001, <https://doi.org/10.7567/APEX.7.091001>.
- [13] M. Velazquez-Rizo, M.A. Najmi, D. Iida, P. Kirilenko, K. Ohkawa, Microstructural analysis of N-polar InGaN directly grown on a ScAlMgO₄ (0001) substrate, *Appl. Phys. Express.* 15 (2022) 065501, <https://doi.org/10.35848/1882-0786/ac6c1a>.
- [14] T. Fukui, Y. Matsuda, M. Matsukura, T. Kojima, M. Funato, Y. Kawakami, Interface formation mechanism of GaN on Al-pretreated ScAlMgO₄ (0001) substrates, *Cryst. Growth Des.* 23 (2023) 2739–2744, <https://doi.org/10.1021/acs.cgd.2c01525>.
- [15] A. Floriduz, E. Matioli, Direct high-temperature growth of single-crystalline GaN on ScAlMgO₄ substrates by metalorganic chemical vapor deposition, *Jpn. J. Appl. Phys.* 61 (2022) 048002, <https://doi.org/10.35848/1347-4065/ac54fe>.
- [16] W. Wang, T. Yan, W. Yang, Y. Zhu, H. Wang, G. Li, N. Ye, Epitaxial growth of GaN films on lattice-matched ScAlMgO₄ substrates, *CrystEngComm.* 18 (2016) 4688–4694, <https://doi.org/10.1039/C6CE01071G>.
- [17] Y. Zheng, W. Wang, X. Li, Y. Li, T. Yan, N. Ye, G. Li, Polarity-controlled GaN epitaxial films achieved via controlling the annealing process of ScAlMgO₄ substrates and the corresponding thermodynamic mechanisms, *J. Phys. Chem. C* 122 (2018) 16161–16167, <https://doi.org/10.1021/acs.jpcc.8b04410>.
- [18] K. Ohnishi, M. Kanoh, T. Tanikawa, S. Kuboya, T. Mukai, T. Matsuoka, Halide vapor phase epitaxy of thick GaN films on ScAlMgO₄ substrates and their self-separation for fabricating freestanding wafers, *Appl. Phys. Express.* 10 (2017) 101001, <https://doi.org/10.7567/APEX.10.101001>.
- [19] T. Araki, S. Kayamoto, Y. Wada, Y. Kuroda, D. Nakayama, N. Goto, M. Deura, S. Mouri, T. Fujii, T. Fukuda, Direct growth of GaN film on ScAlMgO₄ substrate by radio-frequency plasma-excited molecular beam epitaxy, *Appl. Phys. Express.* 16 (2023) 025504, <https://doi.org/10.35848/1882-0786/abc894>.
- [20] T. Ozaki, M. Funato, Y. Kawakami, Red-emitting InGaAl_x–InGaN_y quantum wells grown on lattice-matched InGaAl_x–InGaN_y/ScAlMgO₄ (0001) templates, *Appl. Phys. Express.* 12 (2018) 011007, <https://doi.org/10.7567/1882-0786/aaef4b1>.
- [21] T. Ozaki, Growth of InGaN-Based Emitters on ScAlMgO₄ Substrates for Full Visible Spectral Range, Doctor Thesis, Kyoto University, 2017, <https://doi.org/10.14989/doctor.k20384>.
- [22] V. Ramachandran, R.M. Feenstra, W.L. Sarney, L. Salamanca-Riba, J.E. Northrup, L.T. Romano, D.W. Greve, Inversion of wurtzite GaN(0001) by exposure to magnesium, *Appl. Phys. Lett.* 75 (1999) 808–810, <https://doi.org/10.1063/1.124520>.
- [23] J.E. Northrup, Magnesium incorporation at (0001) inversion domain boundaries in GaN, *Appl. Phys. Lett.* 82 (2003) 2278–2280, <https://doi.org/10.1063/1.1565707>.
- [24] A.K. Viswanath, E.-j. Shin, J.I. Lee, S. Yu, D. Kim, B. Kim, Y. Choi, C.-H. Hong, Magnesium acceptor levels in GaN studied by photoluminescence, *J. Appl. Phys.* 83 (1998) 2272–2275, <https://doi.org/10.1063/1.366985>.
- [25] A. Kumar, W. Yi, J. Uzuhashi, T. Ohkubo, J. Chen, T. Sekiguchi, R. Tanaka, S. Takashima, M. Edo, K. Hono, Influence of implanted mg concentration on defects and mg distribution in GaN, *J. Appl. Phys.* 128 (2020) 065701, <https://doi.org/10.1063/5.0014717>.
- [26] I. Akasaki, H. Amano, H. Murakami, M. Sassa, H. Kato, K. Manabe, Growth of GaN and AlGaN for UV/blue p-n junction diodes, *J. Cryst. Growth* 128 (1993) 379–383, [https://doi.org/10.1016/0022-0248\(93\)90352-W](https://doi.org/10.1016/0022-0248(93)90352-W).
- [27] Y. Hu, C.A. Hernández-Gutiérrez, H.I. Solís-Cisneros, G. Santana, Y. Kudriatsev, J. L. Camas-Anzueto, M. López-López, Blue luminescence origin and Mg acceptor saturation in highly doped zinc-blende GaN with Mg, *J. Alloys. Compd.* 897 (2022) 163133, <https://doi.org/10.1016/j.jallcom.2021.163133>.
- [28] S.M. Knoll, S. Zhang, T.B. Joyce, M.J. Kappers, C.J. Humphreys, M.A. Moram, Growth, microstructure and morphology of epitaxial ScGaN films, *Physica Status Solidi* 209 (2012) 33–40, <https://doi.org/10.1002/pssa.201100158>.
- [29] T. Hanada, H. Tajiri, O. Sakata, T. Fukuda, T. Matsuoka, Characterization of the ScAlMgO₄ cleaving layer by x-ray crystal truncation rod scattering, *J. Appl. Phys.* 123 (2018) 205305, <https://doi.org/10.1063/1.5031024>.
- [30] T. Iwabuchi, Fabrication and Improvement of Device Characteristics of InGaN-based LEDs on Cleaved ScAlMgO₄ Substrates, Doctor thesis, Tohoku University, 2019, <https://tohoku.repo.nii.ac.jp/record/130082/files/190327-Iwabuchi-5600-1.pdf>.
- [31] T. Fukuda, Y. Shiraishi, T. Nanto, T. Fujii, K. Sugiyama, R. Simura, H. Ieichi, K. Tadatomo, Growth of bulk single crystal ScAlMgO₄ boules and GaN films on ScAlMgO₄ substrates for GaN-based optical devices, high-power and high-frequency transistors, *J. Cryst. Growth* 574 (2021) 126286, <https://doi.org/10.1016/j.jcrysgro.2021.126286>.
- [32] T. Ozaki, M. Funato, Y. Kawakami, InGaN-based visible light-emitting diodes on ScAlMgO₄ (0001) substrates, *Appl. Phys. Express.* 8 (2015) 062101, <https://doi.org/10.7567/APEX.8.062101>.
- [33] K. Ohnishi, S. Kuboya, T. Tanikawa, T. Iwabuchi, K. Yamamura, N. Hasuike, H. Harima, T. Fukuda, T. Matsuoka, Reuse of ScAlMgO₄ substrates utilized for halide vapor phase epitaxy of GaN, *Jpn. J. Appl. Phys.* 58 (2019), <https://doi.org/10.7567/1347-4065/ab06ab>, SC1023.
- [34] A. Ueta, H. Ohno, N. Yanagita, N. Ryoki, K. Miyano, A. Ishibashi, M. Nobuoka, High quality nitride semiconductors grown on novel ScAlMgO₄ substrates and their light emitting diodes, *Jpn. J. Appl. Phys.* 58 (2019), <https://doi.org/10.7567/1347-4065/ab06b5>, SC1041.
- [35] T. Fukui, T. Sakaguchi, Y. Matsuda, M. Matsukura, T. Kojima, M. Funato, Y. Kawakami, Metalorganic vapor phase epitaxy of GaN on 2 inch ScAlMgO₄ (0001) substrates, *Jpn. J. Appl. Phys.* 61 (2022) 090904, <https://doi.org/10.35848/1347-4065/ac89e2>.
- [36] R. Takahashi, R. Fujiki, K. Hozo, R. Hiramatsu, M. Matsukura, T. Kojima, D.-P. Han, M. Iwaya, T. Takeuchi, S. Kamiyama, Improvement of 650-nm red-emitting gain0.17n/gain0.38n multiple quantum wells on ScAlMgO₄ (0001) substrate by suppressing impurity diffusion/penetration, *Appl. Phys. Lett.* 120 (2022) 142102, <https://doi.org/10.1063/5.0088250>.
- [37] D.-G. Zheng, S. Min, J. Kim, D.-P. Han, Growth of Ga0.70In0.30N/GaN quantum-wells on a ScAlMgO₄ (0001) substrate with an ex-situ sputtered-AlN buffer layer, *Materials* 17 (2023) 167, <https://doi.org/10.3390/ma17010167>.
- [38] M.A. Najmi, P. Kirilenko, D. Iida, K. Ohkawa, Investigation of n-polar InGaN growth on misoriented ScAlMgO₄ substrates, *Sci. Rep.* 13 (2023) 19332, <https://doi.org/10.1038/s41598-023-46542-w>.
- [39] T. Iwabuchi, S. Kuboya, T. Tanikawa, T. Hanada, R. Katayama, T. Fukuda, T. Matsuoka, Ga-polar GaN film grown by mpcv on cleaved ScAlMgO₄ (0001) substrate with millimeter-scale wide terraces, *Physica Status Solidi* 214 (2017) 1600754, <https://doi.org/10.1002/pssa.201600754>.
- [40] H. Nakane, T. Akiyama, K. Nakamura, T. Ito, Structures and stability of polar GaN thin films on ScAlMgO₄ substrate: an ab initio-based study, *J. Cryst. Growth* 468 (2017) 93–96, <https://doi.org/10.1016/j.jcrysgro.2016.09.019>.
- [41] G. Kresse, J. Furthmüller, Efficiency of ab initio total energy calculations for metals and semiconductors using a plane-wave basis set, *Comput. Mater. Sci.* 6 (1996) 15–50, [https://doi.org/10.1016/0927-0256\(96\)00008-0](https://doi.org/10.1016/0927-0256(96)00008-0).
- [42] G. Kresse, J. Furthmüller, Efficient iterative schemes for ab initio total-energy calculations using a plane-wave basis set, *Phys. Rev. B* 54 (1996) 11169–11186, <https://doi.org/10.1103/PhysRevB.54.11169>.
- [43] J.P. Perdew, K. Burke, M. Ernzerhof, Generalized gradient approximation made simple, *Phys. Rev. Lett.* 77 (1996) 3865–3868, <https://doi.org/10.1103/PhysRevLett.77.3865>.
- [44] Y. Guo, Y. Wang, C. Li, X. Li, Y. Niu, S. Hou, Ab initio calculations on the initial stages of GaN and ZnO growth on lattice-matched ScAlMgO₄ (0001) substrates, *Mater. Res. Express.* 3 (2016) 125903, <https://doi.org/10.1088/2053-1591/3/12/125903>.
- [45] S.B. Zhang, S.-H. Wei, Surface energy and the common dangling bond rule for semiconductors, *Phys. Rev. Lett.* 92 (2004) 086102, <https://doi.org/10.1103/PhysRevLett.92.086102>.
- [46] Y. Yan, S.-H. Wei, Doping asymmetry in wide-bandgap semiconductors: origins and solutions, *Physica Status Solidi* 245 (2008) 641–652, <https://doi.org/10.1002/pssb.200743334>.
- [47] J. Neugebauer, C.G. Van de Walle, Gallium vacancies and the yellow luminescence in GaN, *Appl. Phys. Lett.* 69 (1996) 503–505, <https://doi.org/10.1063/1.117767>.
- [48] C.G. Van de Walle, J. Neugebauer, First-principles calculations for defects and impurities: applications to iii-nitrides, *J. Appl. Phys.* 95 (2004) 3851–3879, <https://doi.org/10.1063/1.1682673>.
- [49] U. Wahl, L.M. Amorim, V. Augustyns, A. Costa, E. David-Bosne, T.A.L. Lima, G. Lippert, J.G. Correia, M.R. da Silva, M.J. Kappers, K. Temst, A. Vantomme, L.M. C. Pereira, Lattice location of mg in GaN: a fresh look at doping limitations, *Phys. Rev. Lett.* 118 (2017) 095501, <https://doi.org/10.1103/PhysRevLett.118.095501>.
- [50] J. Wang, W. Cai, W. Lu, S. Lu, E. Kano, V.C. Agullo, B. Sarkar, H. Watanabe, N. Ikarashi, T. Iwamoto, M. Nakajima, Y. Honda, H. Amano, Observation of 2d-magnesium-intercalated gallium nitride superlattices, *Nature* 631 (2024) 67–72, <https://doi.org/10.1038/s41586-024-07513-x>.
- [51] A.J. Garza, G.E. Scuseria, Predicting band gaps with hybrid density functionals, *J. Phys. Chem. Lett.* 7 (2016) 4165–4170, <https://doi.org/10.1021/acs.jpclett.6b01807>.
- [52] I. Vurgaftman, J.R. Meyer, Band parameters for nitrogen-containing semiconductors, *J. Appl. Phys.* 94 (2003) 3675–3696, <https://doi.org/10.1063/1.1600519>.
- [53] S. Zhang, D. Holec, W.Y. Fu, C.J. Humphreys, M.A. Moram, Tunable optoelectronic and ferroelectric properties in Sc-based iii-nitrides, *J. Appl. Phys.* 114 (2013) 133510, <https://doi.org/10.1063/1.4824179>.

Supporting Information

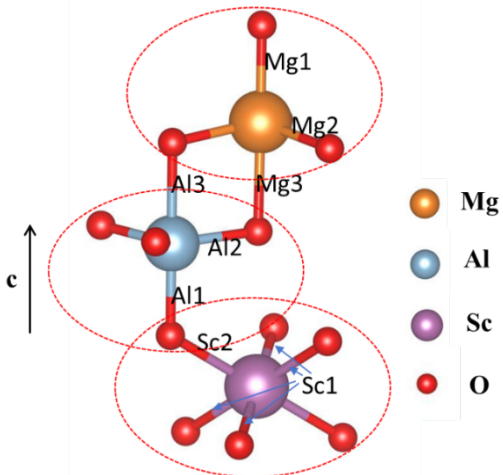


Figure S1 Schematic diagram of the structure and bonding of a chemical formula cyclic unit in SAM.

Table 1 Bond length in bulk SAM

Bond	Bond length/Å
Sc1	2.11
Sc2	2.20
Al1	1.84
Al2	1.76-1.84
Al3	2.25-2.32
Mg3	2.12-2.17
Mg2	1.96-2.05
Mg1	2.02

Table 2 Evidence for the necessity of Mg/Al hybrid modelling in SAM structures

Models	Energy (eV)	Delta Energy (eV)
SAM 1×1 primitive cell*4/bulk	-636.472	1.391
Mg/Al mixed SAM 2×2 primitive cell/bulk	-637.863	
SAM 2×2 pure -Al-surface slab	-628.302	7.869
SAM 2×2 Mg/Al-mixed-surface slab	-636.171	
SAM 2×2 pure-Mg-surface slab	-626.521	9.650
SAM 2×2 Mg/Al-mixed-surface slab	-636.171	
SAM-GaN 2×2 pure-Al-interface slab	-1109.983	0.909
SAM-GaN 2×2 Mg/Al-mixed-interface slab	-1110.892	
SAM-GaN 2×2 pure-Mg-interface slab	-1106.485	4.407
SAM-GaN 2×2 Mg/Al-mixed-interface slab	-1110.892	

Table 3 Values of μ_{Ga} , μ_{N} , and μ_{Mg} at Ga-rich, N-rich, and Mg-rich in the GaN/Mg₂N₃ system.

Atmospheres	μ_{Ga} (eV)	μ_{N} (eV)	μ_{Mg} (eV)
N-rich	-3.84	-8.32(N ₂)	-2.79
Ga-rich	-2.91(Ga)	-9.25	-2.17
Mg-rich	-2.04	-10.28	-1.48 (Mg)

When N-rich, $\mu_N = \frac{1}{2}\mu_{N_2}$; when Ga-rich, $\mu_{\text{Ga}} = \mu_{\text{metal_Ga}}$; and when Mg-rich, $\mu_{\text{Mg}} = \mu_{\text{metal_Mg}}$. The chemical potentials μ_{Ga} , μ_{N} , and μ_{Mg} , satisfy the relationships at all times: $\mu_{\text{Ga}} + \mu_{\text{N}} = \mu_{\text{GaN}}$; $3\mu_{\text{Mg}} + 2\mu_{\text{N}} = \mu_{\text{Mg}_3\text{N}_2}$. Here, μ_{N_2} , $\mu_{\text{metal_Ga}}$, $\mu_{\text{metal_Mg}}$, μ_{GaN} , and $\mu_{\text{Mg}_3\text{N}_2}$ represent the energies of the N₂ molecule, Ga metal, Mg metal, GaN and Mg₃N₂ protocells, respectively.

Table 4 Formation energies of Mg vacancies on various terminal surfaces of SAM.

Terminal surfaces	Perfect energy (eV)	Mg Vacancy energy (eV)	Formation energy (Mg-rich) (eV)	Formation energy (N-rich) (eV)
OSc	-865.821	-864.013	0.33	-0.98
O	-84.6429	-76.7189	6.44	5.13
OMg	-734.246	-732.389	0.38	-0.93
OO	-664.817	-656.267	7.07	5.76
MgO	-636.171	-625.508	9.18	7.87
Mg	-551.528	-548.789	1.26	-0.05
ScO	-943.16	-933.258	8.42	7.11

Table 5 Values of μ_{Ga} , μ_{N} , and μ_{Sc} at Ga-rich, N-rich, and Sc-rich in the GaN/ScN system.

Atmospheres	μ_{Ga} (eV)	μ_{N} (eV)	μ_{Sc} (eV)
N-rich	-3.84	-8.32(N ₂)	-10.09
Ga-rich	-2.91(Ga)	-9.25	-9.16
Sc-rich	0.07	-12.23	-6.18(Sc)

When N-rich, $\mu_N = \frac{1}{2}\mu_{N_2}$; when Ga-rich, $\mu_{\text{Ga}} = \mu_{\text{metal_Ga}}$; and when Sc-rich, $\mu_{\text{Sc}} = \mu_{\text{metal_Sc}}$. The chemical potentials μ_{Ga} , μ_{N} , and μ_{Sc} satisfy the following relationships at all times: $\mu_{\text{Ga}} + \mu_{\text{N}} = \mu_{\text{GaN}}$; $\mu_{\text{Sc}} + \mu_{\text{N}} = \mu_{\text{ScN}}$. Here, μ_{N_2} , $\mu_{\text{metal_Ga}}$, $\mu_{\text{metal_Sc}}$, μ_{GaN} , and μ_{ScN} represent the calculated energies of the N₂ molecule, Ga metal, Sc metal, GaN and ScN protocells, respectively.

Additional Computations

Surface Energy Calculations:

1. Performed initial 2×2 model calculation followed by 1×1 model validation against literature data.
2. Convergence tests were performed on the GaN layer thickness in GaN-SCAM layer modelling using 1×1 supercells, ultimately determining five layers as optimal.

Interface Energy Analysis:

1. As a precautionary measure, we systematically constructed 1×1 interfaces between SAM terminals (all possible terminations) and GaN substrates with varying polarities and atomic alignments. Based on the extensive data calculated from these models, we identified the ScO-, Mg/AlO-, and OMg/Al-terminated interfaces as having the lowest interface energies. This further supports the selection of the most stable surface model for discussing the interface. Subsequent 2×2 calculations with MgAl-mixed SAMs was performed using these three terminal configurations, as detailed in the main text.
2. Explored interfacial atomic arrangements:
 - Investigated energy impacts of Mg/Al distribution patterns near interfaces (Fig. I)
 - Compared fully Mg-terminated, fully Al-terminated, and mixed Mg/Al configurations (Fig. II)
 - Eventually we ruled out the others and settled on the interface atom arrangement, as described in the main text.

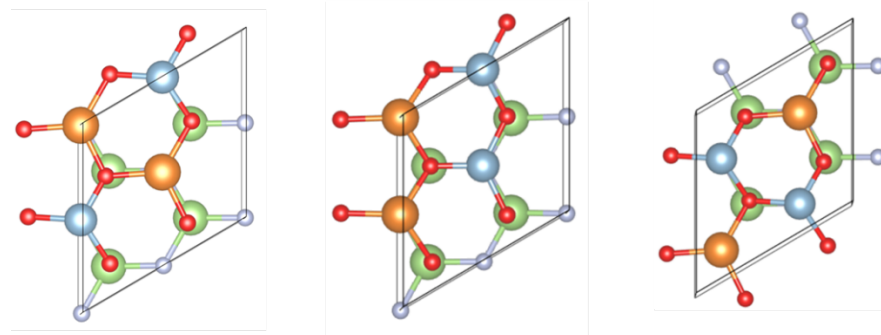


Figure I . Models to calculate interface energy with different Mg/Al distribution.

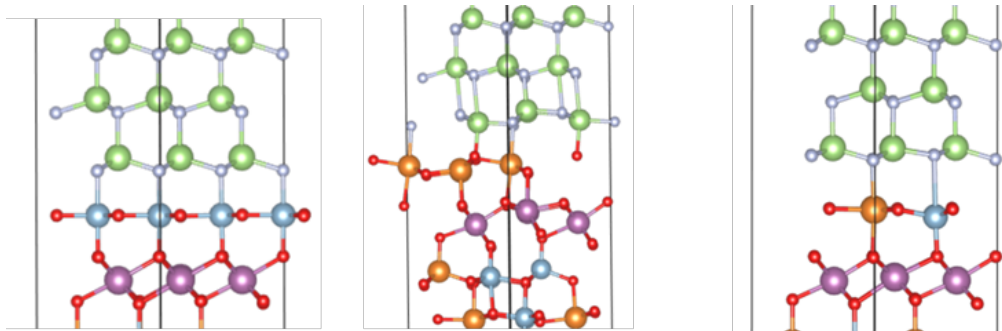


Figure II . Models to calculate interface energy with fully Mg-terminated, fully Al-terminated, and mixed Mg/Al configurations.

Defect Formation Energy Studies:

- Calculated the formation energies of Mg-Ga antisites at different depths in 1×1 models (Fig. III), confirming that only interface-proximal defects need to be considered.

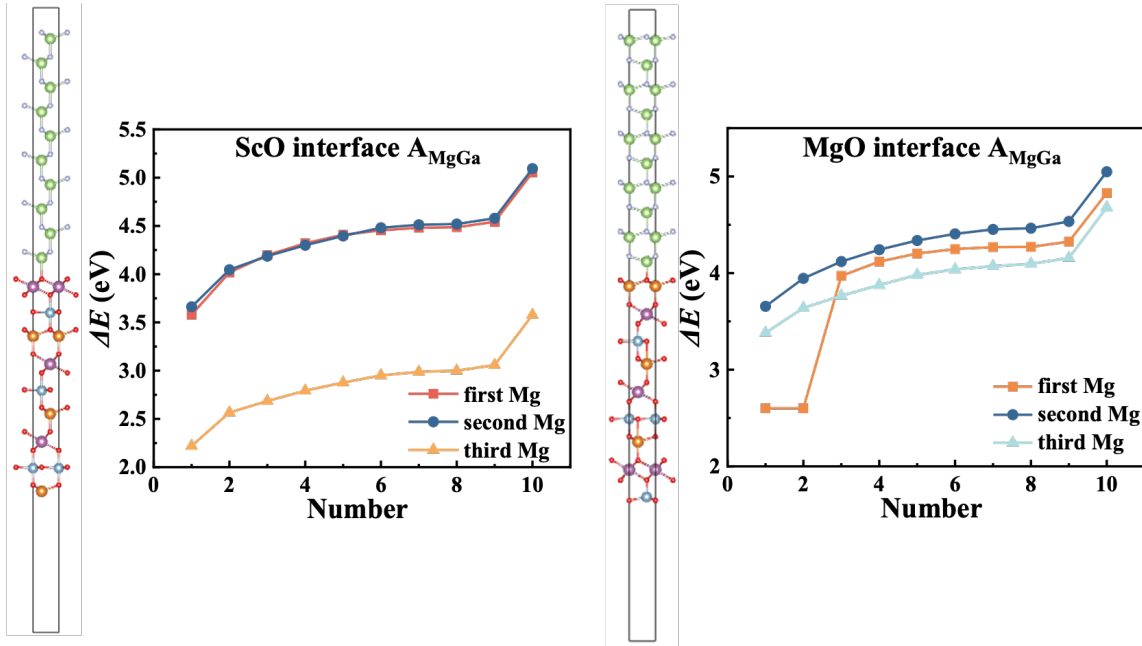


Figure III. Formation energies of Mg-Ga antisites in ScO and MgO structures as a function of GaN depth from the interface.

- Validated the representativeness of the model through comparative studies (see Fig. IV), and established 2×2 mix as the minimal viable model for defect analysis:
 - Compared the formation energies of Mg-Ga antisite across the 1×1 unmix, 2×2 unmix, and 2×2 mix models. The 2×2 mix model exhibited the lowest energy.
 - Observed a slight decrease in formation energy as the model size increased (2×2 mix \rightarrow 3×3 mix \rightarrow 4×4 mix), which is consistent with the expectations from Boltzmann distribution.

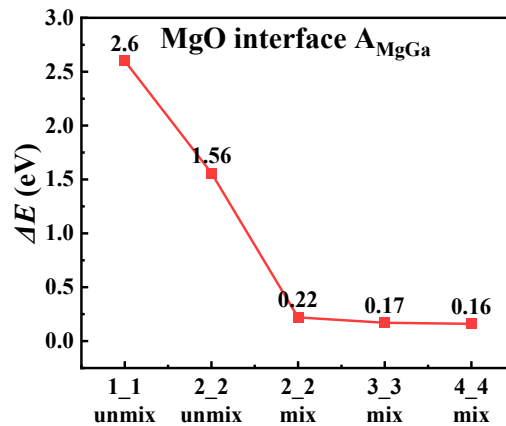


Figure IV. Formation energies of Mg-Ga antisite in different models.

- Demonstrated negligible energy differences (<10 meV) between nearest-neighbor and next-nearest-neighbor exchange sites for the Mg-Ga antisite defect.